Large Tunneling Magnetoresistance in Perpendicularly Magnetized Magnetic Tunnel Junctions Using $Co_{75}Mn_{25}/Mo/Co_{20}Fe_{60}B_{20}$ Multilayers

Tatsuya Yamamoto,[1,*] Tomohiro Ichinose,[1] Jun Uzuhashi,[2] Takayuki Nozaki,[1] Tadakatsu Ohkubo,[2] Kay Yakushiji,[1] Shingo Tamaru,[1] and Shinji Yuasa[1]

[1] *National Institute of Advanced Industrial Science and Technology (AIST), Research Center for Emerging Computing Technologies, Tsukuba, Ibaraki 305-8568, Japan*

[2] *National Institute for Materials Science (NIMS), Tsukuba, Ibaraki 305-0047, Japan*

(Received 3 November 2022; revised 13 January 2023; accepted 17 January 2023; published 7 February 2023)

We study the magnetic and electrical transport properties of magnetic tunnel junctions (MTJs) consisting of a $Co_{75}Mn_{25}/Mo/Co_{20}Fe_{60}B_{20}$ multilayer prepared using a mass-production-compatible magnetron sputtering system. The $Co_{75}Mn_{25}/Mo/Co_{20}Fe_{60}B_{20}$ multilayer sandwiched between two MgO layers exhibits remarkable perpendicular magnetic anisotropy, and a uniaxial magnetic anisotropy constant as large as 0.2 MJ/m^3 is achieved by optimizing the $Co_{75}Mn_{25}$ layer thickness as well as the annealing temperature. The current-in-plane tunneling measurement reveals a large tunneling magnetoresistance of over 100% in perpendicularly magnetized MTJs. These experimental results indicate the applicability of $Co_{75}Mn_{25}$ alloy for magnetic random access memory devices.

DOI: 10.1103/PhysRevApplied.19.024020

I. INTRODUCTION

Magnetic tunnel junctions (MTJs) using perpendicularly magnetized ferromagnetic layers have been intensively studied to develop high-density and energy-efficient magnetic random access memory (MRAM) devices [1–4]. In terms of MRAM application, a large tunneling magnetoresistance (TMR) is also required to improve the signal-to-noise ratio for a high-speed data readout. Among various MTJ materials, Co-Fe alloys/MgO multilayers are the most promising material combination that enables a large TMR of over 100% [5–7] as well as a large perpendicular magnetic anisotropy (PMA) [8–11]. These remarkable TMR and PMA in Co-Fe alloy/MgO MTJs originate from the coherent spin-polarized tunneling through the (001)-oriented MgO barrier [12,13] and large interfacial PMA due to the hybridization of Fe(Co) 3*d* and O 2*p* orbitals [14,15], respectively. The use of an amorphous Co-Fe-B film enables the fabrication of MTJs with a highly (001)-oriented MgO barrier on a polycrystalline electrode using mass-production-compatible magnetron sputtering processes [9–11]. The Co-Fe-B-based perpendicularly magnetized MTJs (pMTJs) are currently used for state-of-the-art MRAM memory cells. Continued development of MTJ materials remains necessary for next-generation MRAMs including those using spin-orbit torque (SOT) [16–18] and/or the voltage-controlled magnetic anisotropy (VCMA) effect [19–21] to further improve the energy efficiency.

The use of bcc Fe-Co-Mn ternary alloys is an alternative approach for developing high-TMR MTJs [22,23]. The bcc Fe-Co-Mn is a metastable phase that can be obtained from epitaxial growth on single-crystal substrates such as GaAs(001) [24] and MgO(001) [25–27]. An intriguing property of the bcc Fe-Co-Mn is the large magnetic moment that even exceeds the Slater-Pauling limit depending on the alloy composition [27]. This unusual feature comes from the large magnetic moment of Mn atoms, which ferromagnetically aligns to that of Fe and Co atoms. First-principles calculation reveals that the band structure of bcc $Co_{75}Mn_{25}$ alloy near the Fermi level is similar to those of bcc Fe and Co, i.e., the Δ_1 state exists only for the majority spin band at the Fermi level [23]. Kunimatsu *et al.* experimentally demonstrates a large TMR ratio of over 200% in an epitaxial $Co_{75}Mn_{25}/MgO/Co_{75}Mn_{25}$ MTJ prepared on a single-crystal MgO(001) substrate [23]. Therefore, the next step toward practical use is to achieve large PMA in sputter-deposited polycrystalline films. In this paper, we evaluate the magnetic and electrical properties of MTJs consisting of an ultrathin (< 1 nm) $Co_{75}Mn_{25}$ film deposited using a mass-production-compatible magnetron sputtering system. The $Co_{75}Mn_{25}$ ultrathin film deposited on a MgO barrier layer exhibits PMA, and pMTJ films consisting of a $Co_{75}Mn_{25}/Mo/Co_{20}Fe_{60}B_{20}$ multilayer are deposited on 300-mm Si wafers with a polycrystalline electrode.

*yamamoto-t@aist.go.jp

TMR ratios of over 100% are also demonstrated by optimizing the $Co_{75}Mn_{25}$ layer thickness and post-annealing temperature.

II. EXPERIMENT

The MTJ films are prepared on 300-mm Si wafers with a 100-nm-thick thermally oxidized Si layer using an ultrahigh-vacuum magnetron sputtering system manufactured by Tokyo Electron Ltd (TEL-EXIM). After the deposition, the wafers are cut into 20×20 mm^2 square chips then annealed at $T_a = 200 - 380$°C for 1 h in a vacuum. Figure 1 shows a schematic of the MTJ stack along with a representative out-of-plane magnetization curve measured using a vibrating sample magnetometer (VSM). A strong antiferromagnetic coupling in the Co/Pt-based synthetic antiferromagnetic reference layer is obtained using an Ir spacer layer [28]. The Ta/Cu bottom electrode is used to evaluate the TMR as well as the resistance-area product of MTJ films by using the current-in-plane tunneling magnetoresistance (CIPT) technique [29]. The free layer consists of a MgO (2 nm)/$Co_{75}Mn_{25}$ (t nm)/Mo (0.3 nm)/$Co_{20}Fe_{60}B_{20}$ (0.6 nm)/MgO (0.8 nm)/capping layer structure if not otherwise specified. The Mo spacer layer is chosen because Mo exhibits small intermixing with Fe and Co, and large PMA of over 0.3 MJ/m^3 is reported for MgO/Co-Fe-B/Mo/Co-Fe-B/MgO multilayers [30].

A $Co_{75}Mn_{25}$ alloy target is used for depositing the $Co_{75}Mn_{25}$ thin films, and the sputtering rate of $Co_{75}Mn_{25}$, Mo, and $Co_{20}Fe_{60}B_{20}$ are calibrated using x-ray fluorescence (XRF). The compositional ratio in the deposited $Co_{75}Mn_{25}$ films is also determined by XRF to be Co 75.5 at.% versus Mn 24.5 at.%. To quantitatively evaluate the PMA in the MgO/$Co_{75}Mn_{25}$/Mo/$Co_{20}Fe_{60}B_{20}$/MgO multilayer, we carry out vector network analyzer ferromagnetic resonance (VNA-FMR) measurement [31]. Scanning transmission electron microscopy (STEM), nanobeam electron diffraction (NBD), and energy dispersive x-ray spectrometry (EDS) are also carried out using FEI Titan G2 80-200 to investigate the nanostructural properties and atomic distribution of the MTJ. Thin foil specimens for the nanostructural analyses are prepared using a focused ion beam with a scanning electron microscopy system (FEI Helios G4UX) through a standard lift-out method.

III. RESULTS AND DISCUSSION

Figure 2(a) minor magnetization curves obtained from the MTJ films consisting of $Co_{75}Mn_{25}$ (0.8 nm)/Mo (0.3 nm)/$Co_{20}Fe_{60}B_{20}$ (0.6 nm) and $Co_{75}Mn_{25}$ (0.8 nm)/Mo (0.3 nm)/$Co_{75}Mn_{25}$ (0.6 nm) free layers. The MTJ films are annealed at $T_a = 350$°C. The saturation magnetization of the $Co_{75}Mn_{25}$/Mo/$Co_{75}Mn_{25}$ free layer is considerably smaller than that of $Co_{75}Mn_{25}$/Mo/$Co_{20}Fe_{60}B_{20}$ free layer even if the difference in the saturation magnetization between bcc Co-Fe (approximately 2.2 T [32]) and bcc $Co_{75}Mn_{25}$ (approximately 2.0 T [22,26]) is taken into account. Therefore, it is expected that the fcc $Co_{75}Mn_{25}$ phase with a much smaller magnetic moment is formed in the $Co_{75}Mn_{25}$/Mo/$Co_{75}Mn_{25}$ free layer. It should be noted that the saturation field of the $Co_{75}Mn_{25}$/Mo/$Co_{75}Mn_{25}$ free layer (approximately 0.42 T) is smaller than the demagnetizing field (approximately 0.68 T), which reveals finite positive PMA at the MgO/$Co_{75}Mn_{25}$ interface. As shown in Fig. 2(a), the use of $Co_{20}Fe_{60}B_{20}$ instead of the upper $Co_{75}Mn_{25}$ substantially enhances PMA and saturation magnetization, enabling a perpendicularly magnetized $Co_{75}Mn_{25}$

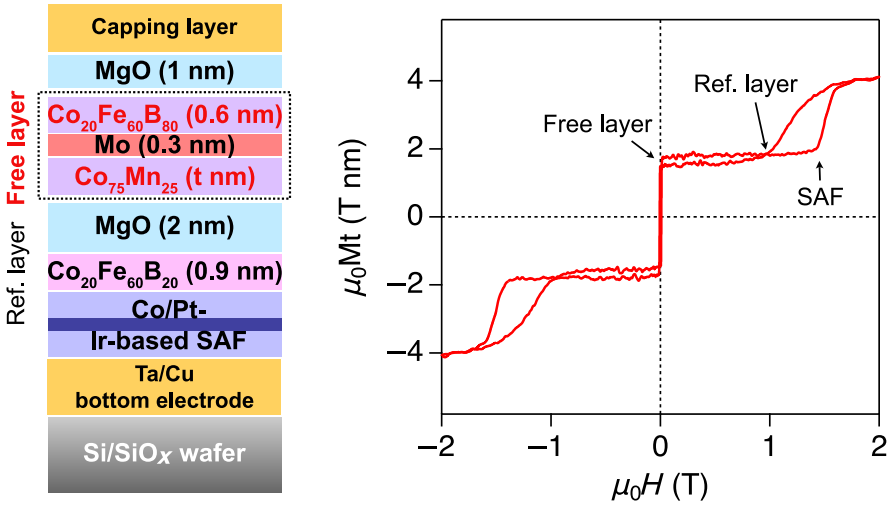

FIG. 1. Schematic illustration of MTJ and representative magnetization curve obtained from MTJ consisting of a $Co_{75}Mn_{25}$ (0.8 nm)/Mo (0.3 nm)/$Co_{20}Fe_{60}B_{20}$ (0.6 nm) multilayer annealed at 350°C. Magnetization curve is measured under application of out-of-plane magnetic field.

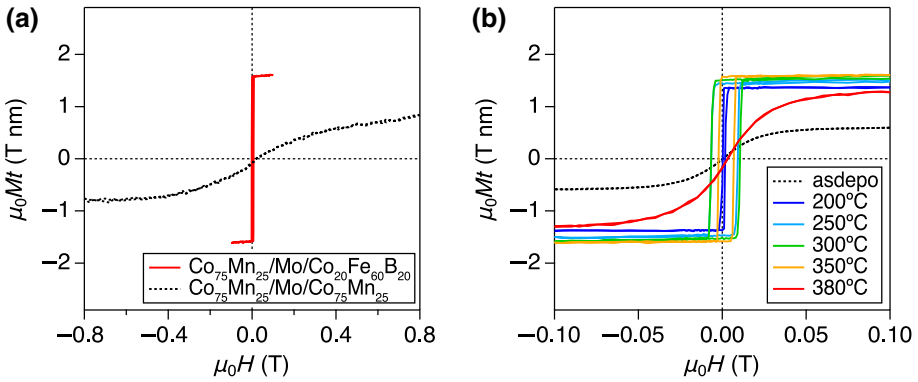

FIG. 2. Out-of-plane minor magnetization curves representing the magnetization process of the free layer: (a) $Co_{75}Mn_{25}$ (0.8 nm)/Mo (0.3 nm)/$Co_{20}Fe_{60}B_{20}$ (0.6 nm) and $Co_{75}Mn_{25}$ (0.8 nm)/Mo (0.3 nm)/$Co_{75}Mn_{25}$ (0.6 nm) free layers annealed at $T_a = 350°C$, and (b) $Co_{75}Mn_{25}$ (0.8 nm)/Mo (0.3 nm)/$Co_{20}Fe_{60}B_{20}$ (0.6 nm) free layer annealed at various T_a.

layer. Therefore, it is considered that the formation of the fcc $Co_{75}Mn_{25}$ phase is effectively prevented in the $Co_{75}Mn_{25}$/Mo/$Co_{20}Fe_{60}B_{20}$ multilayer.

Figure 2(b) displays minor magnetization curves obtained from the $Co_{75}Mn_{25}$ (0.8 nm)/Mo (0.3 nm)/$Co_{20}Fe_{60}B_{20}$ (0.6 nm) free layer annealed at different T_a. Note that all these MTJ films including the as-prepared one underwent a thermal treatment at 80°C for about 3 min during the wafer-cut process. The as-prepared $Co_{75}Mn_{25}$/Mo/$Co_{20}Fe_{60}B_{20}$ free layer has an in-plane easy axis and exhibits a small saturation magnetization, indicating that the $Co_{75}Mn_{25}$ layer is dominated by the paramagnetic phase(s). Interestingly, annealing at $T_a \geq$ 200°C leads to a remarkable enhancement in the saturation magnetization. This suggests that the $Co_{75}Mn_{25}$ layer crystallizes into the ferromagnetic bcc phase upon annealing. The $Co_{75}Mn_{25}$/Mo/$Co_{20}Fe_{60}B_{20}$ free layer also exhibits perpendicular magnetization for 250°C $\leq T_a \leq$ 350°C. Annealing at a higher T_a degrades both the PMA and saturation magnetization.

Figure 3(a) displays a bright field (BF-)STEM image of the MTJ films consisting of the $Co_{75}Mn_{25}$ (0.8 nm)/Mo (0.3 nm)/$Co_{20}Fe_{60}B_{20}$ (0.6 nm) multilayer after annealing at $T_a = 350°C$. The BF-STEM image as well as the NBD patterns [Fig. 3(b)] reveal the formation of (001)-oriented MgO layer and the partial crystallization of the $Co_{75}Mn_{25}$/Mo/$Co_{20}Fe_{60}B_{20}$ multilayer after annealing at $T_a = 350°C$. Although the crystalline structure of the $Co_{75}Mn_{25}$/Mo/$Co_{20}Fe_{60}B_{20}$ multilayer cannot be distinguished from the BF-STEM image and the NBD patterns shown in Fig. 3, the large saturation magnetization revealed from the VSM measurements suggests the bcc crystallization of $Co_{75}Mn_{25}$. Figure 3(c) displays the EDS elemental line profile obtained from the rectangle region drawn in Fig. 3(a) along the direction of the arrow. Due to the considerable film roughness, the atomic ratio at each position may contain a certain amount of uncertainty. However, it is noteworthy that we achieve perpendicular magnetization using a Co-rich ferromagnet, which is beneficial for improving the VCMA efficiency [33–35]. Note

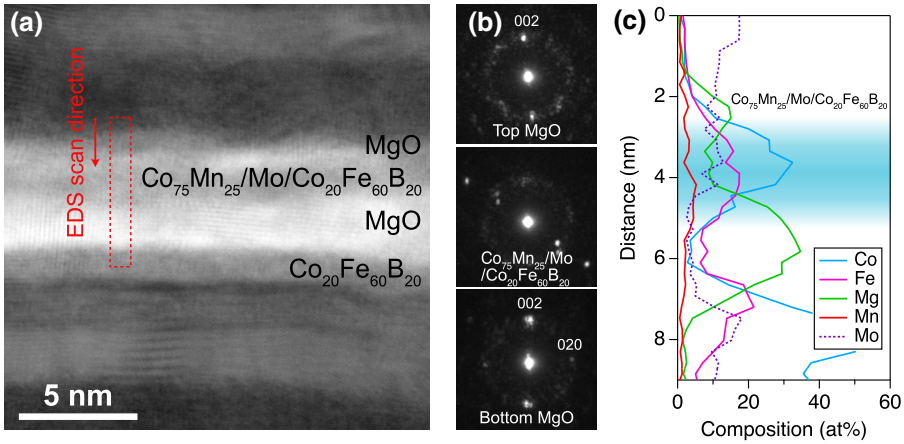

FIG. 3. Nanostructural analysis results on $Co_{75}Mn_{25}$ (0.8 nm)/Mo (0.3 nm)/$Co_{20}Fe_{60}B_{20}$ (0.6 nm) free layer annealed at $T_a = 350°C$: (a) BF-STEM image, (b) NBD patterns, and (c) EDS elemental line profile.

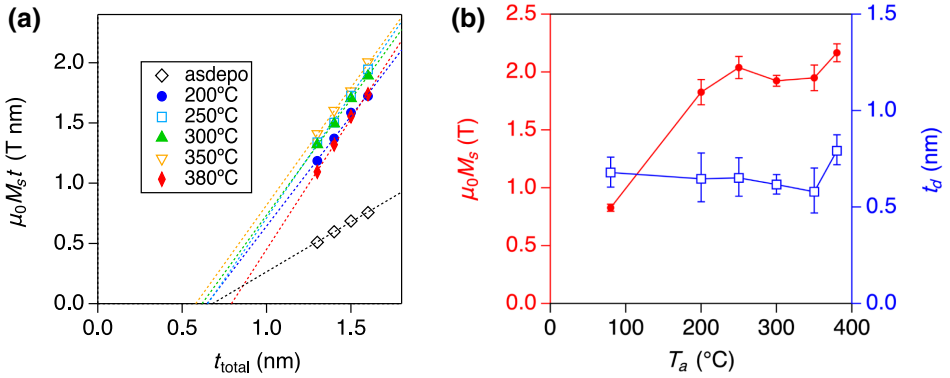

FIG. 4. Post-annealing effect on $Co_{75}Mn_{25}$/Mo/$Co_{20}Fe_{60}B_{20}$ free layer: (a) $Co_{75}Mn_{25}$ thickness dependence of $\mu_0 M_s t$, and (b) T_a dependence of $\mu_0 M_s$ and t_d. $t_{total} = t + 0.6$.

also that there is no significant change in the line profile of Mn atoms associated with the annealing, i.e., most Mn atoms remain on top of the MgO barrier layer. The interfacial Mn atoms can exhibit a large PMA as well as VCMA. [36].

To estimate the saturation magnetization of $Co_{75}Mn_{25}$ in our MTJ films, we evaluate the $\mu_0 M_s t_{total}$ values by varying the $Co_{75}Mn_{25}$ thickness t in the MTJs, and the results are shown in Fig. 4(a). The total free layer thickness, t_{total}, is defined as the sum of the $Co_{75}Mn_{25}$ and $Co_{20}Fe_{60}B_{20}$ thicknesses, i.e., $t_{total} = t + 0.6$ nm. The slope and t_{total} intercept of linear fits to the experimental data correspond to the saturation magnetization $\mu_0 M_s$ and dead layer thickness in the $Co_{75}Mn_{25}$/Mo/$Co_{20}Fe_{60}B_{20}$ stack t_d, respectively. Figure 4(b) summarizes the estimated values of $\mu_0 M_s$ and t_d as a function of T_a. Annealing at $T_a \geq 200°C$ remarkably enhanced the saturation magnetization, and $\mu_0 M_s$ values as large as 2.0 T are obtained for $250°C \leq T_a \leq 350°C$. For this T_a range, the t_d value is constant around 0.6 nm. These results suggest that the ferromagnetic (bcc) phase is stabilized in the $Co_{75}Mn_{25}$ layer for $250°C \leq T_a \leq 350°C$. Annealing at $T_a = 380°C$ led to a slight increase in t_d, which can be explained by the formation of paramagnetic fcc phase [23] and interlayer atomic diffusion in the $Co_{75}Mn_{25}$/Mo/$Co_{20}Fe_{60}B_{20}$ stack. These magnetic phase transition in $Co_{75}Mn_{25}$ may be used to further improve the efficiencies of VCMA- and SOT-driven magnetization switching by replicating the phase transition using the Joule heating and/or an electric field.

Figure 5(a) displays the FMR frequency f_0 determined from the VNA-FMR measurements as a function of the applied out-of-plane field $\mu_0 H$. For all MTJ films, the f_0 linearly increases with increasing $\mu_0 H$; thus, one can estimate from the linear dependence the saturation field H_k as well as PMA energy density K_u ($= M_s H_k/2$). Figure 5(b) summarizes the T_a dependence of K_u for the MTJ films with different t. Regardless of t, K_u maximizes at around $T_a = 250 - 300°C$, and the largest K_u of 0.2 MJ/m^3 is achieved for $T_a = 300°C$ with $t = 0.7$ nm. Although this K_u value is smaller than that reported for MgO/Co-Fe-B/Mo/Co-Fe-B/MgO [30,37] and Mo buffer/Co-Fe-B/MgO multilayers [38–40], it is comparable to the standard Ta buffer/Co-Fe-B/MgO junctions [10,35].

Finally, we discuss the TMR characteristics of the $Co_{75}Mn_{25}$/Mo/$Co_{20}Fe_{60}B_{20}$ MTJ films determined from CIPT measurements under an out-of-plane magnetic field.

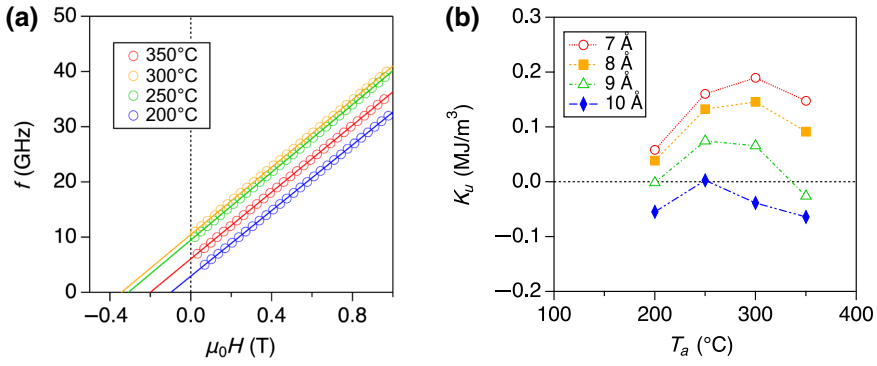

FIG. 5. VNA-FMR measurement results: (a) FMR frequency as function of applied out-of-plane field. (b) K_u values estimated from H_k and M_s values.

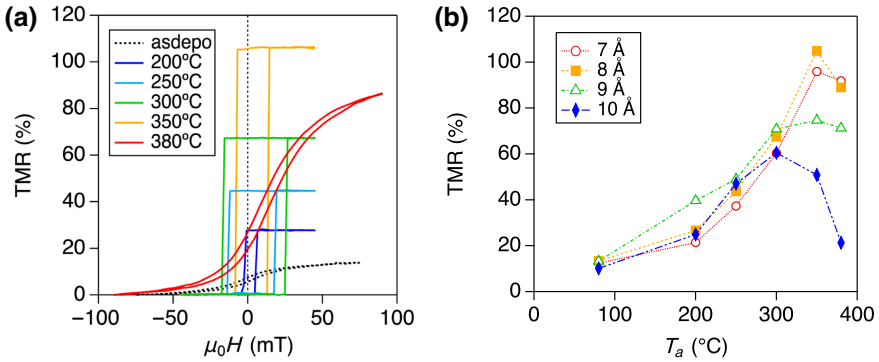

FIG. 6. CIPT measurement results: (a) TMR as function of applied out-of-plane field. (b) TMR as function of T_a.

Figure 6(a) displays the TMR curves obtained from the $Co_{75}Mn_{25}$ (0.8 nm)/Mo (0.3 nm)/$Co_{20}Fe_{60}B_{20}$ (0.6 nm) MTJ films annealed at various T_a. In accordance with the VSM and FMR measurement results, square-shaped TMR curves, which represent the switching of the perpendicularly magnetized $Co_{75}Mn_{25}$/Mo/$Co_{20}Fe_{60}B_{20}$ free layer are obtained for $T_a = 200 - 350$°C. The $Co_{75}Mn_{25}$/Mo/$Co_{20}Fe_{60}B_{20}$ MTJ film exhibits a large TMR ratio of over 100% after annealing at $T_a = 350$°C. Figure 6(b) displays the T_a dependence of the TMR ratio determined from the CIPT measurement. The largest TMR of 105% is obtained for the $Co_{75}Mn_{25}$ (0.8 nm)/Mo (0.3 nm)/$Co_{20}Fe_{60}B_{20}$ (0.6 nm) MTJ film annealed at $T_a =$ 350°C. Although this TMR ratio is smaller than that reported for an in-plane-magnetized MTJ using epitaxially grown bcc-$Co_{75}Mn_{25}$ electrodes [22,23], it should be stressed that we obtain a large TMR ratio of over 100% in *perpendicularly magnetized* MTJ films using *polycrystalline* $Co_{75}Mn_{25}$ electrodes. Note that the smaller TMR for the MTJ films consisting of 9- and 10-Å-thick $Co_{75}Mn_{25}$ films is due to the unsaturated magnetic moment in the $Co_{75}Mn_{25}$/Mo/$Co_{20}Fe_{60}B_{20}$ layer with insufficient PMA. Further enhancements in the TMR as well as PMA will be readily achieved by improving the flatness of the bottom electrode.

IV. SUMMARY

To summarize, we study the magnetic and electrical transport properties of MTJ films consisting of $Co_{75}Mn_{25}$/Mo/$Co_{20}Fe_{60}B_{20}$ multilayers prepared on a polycrystalline electrode. The $Co_{75}Mn_{25}$/Mo/$Co_{20}Fe_{60}B_{20}$ multilayers exhibited remarkable PMA and a fairly large K_u of 0.2 MJ/m^3 is achieved after annealing at $T_a =$ 300°C. A TMR ratio of 105% is also obtained for perpendicularly magnetized $Co_{75}Mn_{25}$/Mo/$Co_{20}Fe_{60}B_{20}$ MTJ films. These experimental results will contribute to the development of advanced MRAMs including voltage-controlled MRAM and SOT-MRAM.

ACKNOWLEDGMENTS

The authors thank T. Nozaki, M. Konoto, A. Sugihara, S. Tsunegi, Y. Hibino, M. Endo, H. Ohmori, Y. Higo, Y. Kageyama, and M. Hosomi for their fruitful discussions, and E. Usuda, M. Toyoda, and K. Suzuki for assisting with the experiments. This work is based on results obtained from a project, JPNP20017, commissioned by the New Energy and Industrial Technology Development Organization (NEDO), Japan.

[1] H. Yoda *et al.*, High efficient spin transfer torque writing on perpendicular magnetic tunnel junctions for high density mrams, Curr. Appl. Phys. **10**, e87 (2010).

[2] D. C. Worledge, G. Hu, David W. Abraham, P. L. Trouilloud, and S. Brown, Development of perpendicularly magnetized Ta—CoFeB—MgO-based tunnel junctions at ibm, J. Appl. Phys. **115**, 172601 (2014).

[3] K. Ando, S. Fujita, J. Ito, S. Yuasa, Y. Suzuki, Y. Nakatani, T. Miyazaki, and H. Yoda, Spin-transfer torque magnetoresistive random-access memory technologies for normally off computing, J. Appl. Phys. **115**, 172607 (2014).

[4] L. Thomas, G. Jan, J. Zhu, H. Liu, Y.-J. Lee, S. Le, R.-Y. Tong, K. Pi, Y.-J. Wang, D. Shen, R. He, J. Haq, J. Teng, V. Lam, K. Huang, T. Zhong, T. Torng, and P.-K. Wang, Perpendicular spin transfer torque magnetic random access memories with high spin torque efficiency and thermal stability for embedded applications, J. Appl. Phys. **115**, 172615 (2014).

[5] S. S. P. Parkin, C. Kaiser, A. Panchula, P. M. Rice, B. Hughes, M. Samant, and S.-H. Yang, Giant tunneling magnetoresistance at room tempereature with MgO (100) tunnel barriers, Nat. Mater. **3**, 862 (2004).

[6] S. Yuasa, T. Nagahama, A. Fukushima, Y. Suzuki, and K. Ando, Giant room-temperature magnetoresistance in single-crystal Fe/MgO/Fe magnetic tunnel junctions, Nat. Mater. **3**, 868 (2004).

[7] D. D. Djayaprawira, K. Tsunekawa, M. Nagai, H. Maehara, S. Yamagata, N. Watanabe, S. Yuasa, Y. Suzuki, and K. Ando, 230% room-temperature magnetoresistance in CoFeB/MgO/CoFeB magnetic tunnel junctions, Appl. Phys. Lett. **86**, 092502 (2005).

[8] T. Shinjo, S. Hine, and T. Takada, Mössbauer spectra of ultrathin Fe films coated by MgO, J. de Phys. **40**, C2–86 (1979).

[9] S. Yakata, H. Kubota, Y. Suzuki, K. Yakushiji, A. Fukushima, S. Yuasa, and K. Ando, Influence of perpendicular magnetic anisotropy on spin-transfer switching current in CoFeB/MgO/CoFeB magnetic tunnel junctions, J. Appl. Phys. **105**, 07D131 (2009).

[10] S. Ikeda, K. Miura, H. Yamamoto, K. Mizunuma, H. D. Gan, M. Endo, S. Kanai, J. Hayakawa, F. Matsukura, and H. Ohno, A perpendicular-anisotropy CoFeB-MgO magnetic tunnel junction, Nat. Mater. **9**, 721 (2010).

[11] H. Kubota, S. Ishibashi, T. Saruya, T. Nozaki, A. Fukushima, K. Yakushiji, K. Ando, Y. Suzuki, and S. Yuasa, Enhancement of perpendicular magnetic anisotropy in FeB free layers using a thin MgO cap layer, J. Appl. Phys. **111**, 07C723 (2012).

[12] J. Mathon and A. Umerski, Theory of tunneling magnetoresistance of an epitaxial Fe/MgO/Fe (001) junction, Phys. Rev. B **63**, 220403 (2001).

[13] W. H. Butler, X.-G. Zhang, T. C. Schulthess, and J. M. MacLaren, Spin-dependent tunneling conductance of Fe—MgO—Fe sandwiches, Phys. Rev. B **63**, 054416 (2001).

[14] H. X. Yang, M. Chshiev, B. Dieny, J. H. Lee, A. Manchon, and K. H. Shin, First-principles investigation of the very large perpendicular magnetic anisotropy at Fe—MgO and Co—MgO interfaces, Phys. Rev. B **84**, 054401 (2011).

[15] J. Okabayashi, J. W. Koo, H. Sukegawa, S. Mitani, Y. Takagi, and T. Yokoyama, Perpendicular magnetic anisotropy at the interface between ultrathin Fe film and MgO studied by angular-dependent *X*-ray magnetic circular dichroism, Appl. Phys. Lett. **105**, 122408 (2014).

[16] A. Manchon, J. Železný, I. M. Miron, T. Jungwirth, J. Sinova, A. Thiaville, K. Garello, and P. Gambardella, Current-induced spin-orbit torques in ferromagnetic and antiferromagnetic systems, Rev. Mod. Phys. **91**, 035004 (2019).

[17] I. M. Miron, K. Garello, G. Gaudin, P.-J. Zermatten, M. V. Costache, S. Auffret, S. Bandiera, B. Rodmacq, A. Schuhl, and P. Gambardella, Perpendicular switching of a single ferromagnetic layer induced by in-plane current injection, Nature **476**, 189 (2011).

[18] L. Liu, C.-F. Pai, Y. Li, H. W. Tseng, D. C. Ralph, and R. A. Buhrman, Spin-torque switching with the giant spin Hall effect of tantalum, Science **336**, 555 (2012).

[19] T. Nozaki, T. Yamamoto, S. Miwa, M. Tsujikawa, M. Shirai, S. Yuasa, and Y. Suzuki, Recent progress in the voltage-controlled magnetic anisotropy effect and the challenges faced in developing voltage-torque MRAM, Micromachines **10**, 327 (2019).

[20] Y. Shiota, T. Nozaki, F. Bonell, S. Murakami, T. Shinjo, and Y. Suzuki, Induction of coherent magnetization switching in a few atomic layers of FeCo using voltage pulses, Nat. Mater. **11**, 39 (2012).

[21] S. Kanai, M. Yamanouchi, S. Ikeda, Y. Nakatani, F. Matsukura, and H. Ohno, Electric field-induced magnetization reversal in a perpendicular-anisotropy CoFeB-MgO magnetic tunnel junction, Appl. Phys. Lett. **101**, 122403 (2012).

[22] K. Kunimatsu, T. Tsuchiya, T. Roy, K. Elpjick, T. Ichinose, M. Tsujikawa, A. Hirohata, M. Shirai, and S. Mizukami, Fabrication of magnetic tunnel junctions with a metastable bcc Co_3Mn disordered alloy as a bottom electrode, Jpn. J. Appl. Phys. **58**, 080908 (2019).

[23] K. Kunimatsu, T. Tsuchiya, T. Roy, K. Elpjick, T. Ichinose, M. Tsujikawa, A. Hirohata, M. Shirai, and S. Mizukami, Magnetic tunnel junctions with metastable bcc Co_3Mn electrodes, Appl. Phys. Express **13**, 083007 (2020).

[24] D. Wu, G. L. Liu, C. Jing, Y. Z. Wu, D. Loison, G. S. Dong, and X. F. Jin, Magnetic structure of $Co_{1-x}Mn_x$ alloys, Phys. Rev. B **63**, 214403 (2001).

[25] Y. U. Idzerda, H. Bhatkar, and E. Arenholz, Moment mapping of body-centered-cubic Fe_xMn_{1-x} alloy films on MgO(001), J. Appl. Phys. **117**, 17A721 (2015).

[26] R. J. Snow, H. Bhatkar, A. T. N'Diaye, E. Arenholz, and Y. U. Idzerda, Enhanced moments in bcc $Co_{1-x}Mn_x$ on MgO(001), J. Magn. Magn. Mater. **419**, 490 (2016).

[27] R. J. Snow, H. Bhatkar, A. T. N'Diaye, E. Arenholz, and Y. U. Idzerda, Large moments in bcc $Fe_xCo_yMn_z$ ternary alloy thin films, Appl. Phys. Lett. **112**, 072403 (2018).

[28] K. Yakushiji, A. Sugihara, A. Fukushima, H. Kubota, and S. Yuasa, Very strong antiferromagnetic interlayer exchange coupling with iridium spacer layer for perpendicular magnetic tunnel junctions, Appl. Phys. Lett. **110**, 092406 (2017).

[29] D. C. Worledge and P. L. Trouilloud, Magnetoresistance measurement of unpatterned magnetic tunnel junction wafers by current-in-plane tunneling, Appl. Phys. Lett. **83**, 84 (2005).

[30] H. Cheng, J. Chen, S. Peng, B. Zhang, Z. Wang, D. Zhu, K. Shi, S. Eimer, X. Wang, Z. Guo, Y. Xu, D. Xiong, K. Cao, and W. Zhao, Giant perpendicular magnetic anisotropy in Mo-based double-interface free layer structure for advanced magnetic tunnel junctions, Adv. Electron. Mater. **6**, 2000271 (2020).

[31] S. Tamaru, T. Yamamoto, T. Onuma, N. Kikuchi, and S. Okamoto, Development of a high-sensitivity VNA-FMR spectrometer with field modulation detection and its application to magnetic characterization, Electron. Comm. Jpn **104**, e12320 (2021).

[32] P. H. Dederichs, R. Zeller, H. Akai, and H. Ebert, Ab-initio calculations of the electronic structure of impurities and alloys of ferromagnetic transition metals, J. Magn. Magn. Mater. **100**, 241 (1991).

[33] T. Nozaki, M. Endo, M. Tsujikawa, T. Yamamoto, T. Nozaki, M. Konoto, H. Ohmori, Y. Higo, H. Kubota, A. Fukushima, M. Hosomi, M. Shirai, Y. Suzuki, and S. Yuasa, Voltage-controlled magnetic anisotropy in an ultrathin Ir-doped Fe layer with a CoFe termination layer, APL Mater. **8**, 011108 (2020).

[34] T. Yamamoto, T. Nozaki, H. Imamura, Y. Shiota, S. Tamaru, K. Yakushiji, H. Kubota, A. Fukushima, Y. Suzuki, and S. Yuasa, Improvement of write error rate in voltage-driven magnetization switching, J. Phys. D: Appl. Phys. **52**, 164001 (2019).

[35] T. Yamamoto, T. Nozaki, K. Yakushiji, S. Tamaru, H. Kubota, A. Fukushima, and S. Yuasa, Perpendicular magnetic anisotropy and its voltage control in MgO/CoFeB/MgO

junctions with atomically thin Ta adhesion layers, Acta. Mater. **216**, 117097 (2021).

[36] K. Z. Suzuki, S. Kimura, H. Kubota, and S. Mizukami, Magnetic tunnel junctions with a nearly zero moment manganese nanolayer with perpendicular magnetic anisotropy, ACS Appl. Mater. Interfaces **10**, 43305 (2018).

[37] T. Yamamoto, T. Ichhinose, J. Uzuhashi, T. Nozaki, T. Ohkubo, K. Yakushiji, S. Tamaru, H. Kubota, A. Fukushima, K. Hono, and S. Yuasa, Perpendicular magnetic anisotropy and its voltage control in MgO/CoFeB/Mo/CoFeB/MgO junctions, J. Phys. D: Appl. Phys. **55**, 275003 (2022).

[38] T. Liu, Y. Zhang, J. W. Cai, and H. Y. Pan, Thermally robust Mo/CoFeB/MgO trilayers with strong perpendicular magnetic anisotropy, Sci. Rep. **4**, 5895 (2014).

[39] H. Almasi, D. Reifsnyder Hickey, T. Newhouse-lllige, M. Xu, M. R. Rosales, S. Nahar, J. T. Held, K. A. Mkhoyan, and W. G. Wang, Enhanced tunneling magnetoresistance and perpendicular magnetic anisotropy in Mo/CoFeB/MgO magnetic tunnel junctions, Appl. Phys. Lett. **106**, 222409 (2015).

[40] B. Fang, X. Zhang, B. S. Zhang, Z. M. Zeng, and J. W. Cai, Tunnel magnetoresistance in thermally robust Mo/CoFeB/MgO tunnel junction with perpendicular magnetic anisotropy, AIP Adv. **5**, 067116 (2015).